A Molecularly Informed Field-Theoretic Study of the Complexation of Polycation PDADMA with Mixed Micelles of Sodium Dodecyl Sulfate and Ethoxylated Surfactants

My Nguyen[1†], Kevin Shen[1,5†], Nicholas Sherck[2], Stephan Köhler[3], Rohini Gupta[4], Kris T. Delaney[5], M. Scott Shell[1*], Glenn H. Fredrickson[1,5,6*]

[1*]Department of Chemical Engineering, University of California, Santa Barbara, 93106, California, United States.
[2]BASF Corporation, Iselin, 08830, New Jersey, United States.
[3]BASF SE, Ludwigshafen am Rhein, 67056, Germany.
[4]California Research Alliance (CARA) by BASF, Berkeley, 94720, California, United States.
[5*]Materials Research Laboratory, University of California, Santa Barbara, 93106, California, United States.
[6*]Department of Materials, University of California, Santa Barbara, 93106, California, United States.

*Corresponding author(s). E-mail(s): shell@ucsb.edu; ghf@ucsb.edu;
Contributing authors: my@ucsb.edu; kevinshen@ucsb.edu; nicholas.sherck@basf.com; stephan.a.koehler@basf.com; rohini.gupta@basf.com; kdelaney@mrl.ucsb.edu;
†These authors contributed equally to this work.

Abstract

The self-assembly and phase separation of mixtures of polyelectrolytes and surfactants is important to a range of applications, from formulating personal care products to drug encapsulation. In contrast to systems of oppositely charged polyelectrolytes, in polyelectrolyte-surfactant systems the surfactants micellize into structures that are highly responsive to solution conditions. In this work we examine how the morphology of micelles and degree of polyelectrolyte adsorption dynamically change upon varying the mixing ratio of charged and neutral surfactants. Specifically, we consider a solution of the cationic polyelectrolyte polydiallyldimethylammonium (PDADMA), anionic surfactant sodium dodecyl sulfate (SDS), neutral ethoxylated surfactants (C_mEO_n), sodium chloride salt, and water. To capture the chemical specificity of these species we leverage recent developments in constructing molecularly informed field theories *via* coarse-graining from all-atom simulations. Our results show how changing the surfactant mixing ratios and the identity of the nonionic surfactant modulates micelle size and surface charge, and as a result dictates the degree of polyelectrolyte adsorption. These results are in semi-quantitative agreement with experimental observations on the same system.

Keywords: bottom-up coarse-graining, field theory, micelle, surfactant, polyelectrolyte, turbidity, complexation

1 Introduction

Solutions of polyelectrolytes and surfactants underpin many applications covering personal care products [1–5], food products [6–8], and drug encapsulation [9–11]. These systems feature an interesting range of self-assembly and phase behaviors, driven by the interplay of hydrophobic and electrostatic interactions [12–16]. Additionally, polyelectrolyte-surfactant systems are often highly multi-component, featuring at least one polyelectrolyte, a mixture of both neutral and ionic surfactants, cationic and anionic salt species, and water, with many parameters (composition, specific chemical species, molecular weight, temperature, etc.) that can be tuned to achieve desired properties [17–19]. The emergent self-assembly and phase behavior sets a range of rheological properties such as viscosity, lubrication, foamability, and wettability that are key performance targets in formulation design [20, 21].

There is a significant number of experimental works on the behavior of polyelectrolyte-surfactant mixtures. In polyelectrolyte-free solutions of surfactants, the critical micelle concentration (CMC) describes the onset of surfactant self-assembly into micelles [14, 22]. In the presence of polymers or polyelectrolytes, there is usually a critical aggregation concentration (CAC) that precedes the CMC, where attractions between polymer and surfactant enables the formation of aggregates at concentrations lower than the surfactant's intrinsic CMC [23]; these aggregates are also referred to as complexes [24]. Hydrophobic polymers are expected to partition to the core of the resulting aggregates and micelles, while charged polymers typically decorate the surfaces of ionic surfactant aggregates and micelles [14, 17, 25, 26]. At higher concentrations, aggregates and micelles are known to undergo morphological changes into cylindrical micelles, spherical vesicles, lamellar structures, precipitates, and gels [27–31]. These structures in turn can be highly sensitive to the chemistry of the employed polyelectrolytes, surfactants, and salt [13, 18, 29, 32].

Mixtures of polyelectrolytes with oppositely charged micelles can also undergo phase separation through complex coacervation [26, 33–36]. This charge-driven phenomenon results in a coacervate phase rich in macroions, and a supernatant phase lean in macroions, and naturally is highly sensitive to factors like the salt concentration, macroion surface charge, and polymer charge density. Complex coacervation is a very general phenomenon such that the macroions can be polyelectrolytes [37], surfactant micelles [26], charged colloids [38, 39], and proteins among others [40–42], and as a result has garnered significant interest across many fields. Out of these various systems, mixtures of micelles with polyelectrolytes are particularly challenging to study and understand because of the propensity of micellar sizes and morphologies to change significantly with solution conditions. Additionally, experimental systems often employ *mixtures* of surfactants in order to tune micelle properties, underscoring the importance of understanding self-assembly [18, 26].

In this work we develop a multiscale modeling framework that directly addresses surfactant self-assembly in the presence of polyelectrolytes, and we focus on experimental studies by Dubin *et al.*[18, 32] In a series of titration and dilution experiments, Dubin and coworkers revealed how polyelectrolyte-surfactant complexation is highly sensitive to polyelectrolyte linear charge density, micelle surface charge density, and the ionic strength of the solution [17, 32, 43]. Additionally, the ratios of polyelectrolytes to surfactants were also shown to affect the resulting self-assembly behavior [18]. Taken together, these observations corroborate the intuition that electrostatic interactions are a primary driving force for the attraction of polyelectrolytes to charged surfactant micelles.

We model one of the systems they studied, featuring the cationic polyelectrolyte polydiallyldimethylammonium (PDADMA), anionic surfactant sodium dodecyl sulfate (SDS), nonionic ethoxylated surfactants (C_mEO_n), sodium chloride salt, and water (Fig. 1). In these studies, SDS surfactant solution was prepared above the CMC, and a mixture of PDADMA and C_mEO_n was isoionically titrated by the SDS micellar solution, thus steadily increasing the molar ratio of charged to neutral surfactants. Turbidity was monitored and demonstrated distinctive changes upon titration with the SDS solution. At modest mole fractions of charged surfactant SDS ($\sim$0.15-0.3) compared to the total surfactant concentration, the turbidity begins gradually increasing corresponding to the onset of the formation of soluble

complexes, before exhibiting a sharp increase indicating a biphasic coacervation regime at higher mole fractions [32]. In addition to quantifying the effects of charge, Dubin and coworkers also demonstrated how changing the nonionic surfactant species C_mEO_n (i.e., by changing the length n of the hydrophilic EO group) quantitatively changes the observed transitions.

While there are numerous theoretical and simulation models of oppositely charged polyelectrolytes [37, 44–51], there is comparatively less theoretical work addressing the complexation of polyelectrolytes with surfactants [24, 25, 31, 52–55]. Directly simulating these systems by molecular dynamics (MD), even coarse-grained MD, is usually confined to relatively small systems. Additionally, the equilibration of micellar structures is itself limited by the slow processes of diffusion, surfactant exchange, and micelle fission and fusion [56–59]. The characteristic time for these processes is easily on the order of μs for common surfactants [60, 61]. Adding slowly equilibrating polymer chains only makes it more difficult to confidently equilibrate the resulting systems. As a result, many molecular dynamics simulations of polyelectrolyte-surfactant systems model the micelles as pre-assembled colloidal particles [39, 62]. Similarly, many theoretical treatments of polyelectrolyte-surfactant mixtures also avoid the difficult equilibration of surfactants into micelles altogether [24], and make approximations such as treating the micelles as spheres with fixed size and charge [24, 63, 64]. In these models, the micelles act as external potentials on the surrounding polyelectrolyte solution, which is in turn modeled using field-theoretic models. Such approaches neglect the self-assembly of surfactants into micelles in order to facilitate evaluation of the mixture phase behavior.

In contrast to modeling micelles as colloids with fixed properties, in this study we explicitly study the self-assembly of surfactants and polyelectrolytes in soluble complexes. We achieve this by developing a *molecularly informed* field-theoretic model based on the strategy outlined in our previous publications (Fig. 1) [65–67]. Briefly, the approach utilizes the field theory to efficiently simulate large, dense systems containing high-molecular-weight species, while providing chemical specificity through small-scale, all-atom simulations. Specifically, we use relative entropy coarse-graining to derive chemically-sensitive coarse-grained interaction parameters from all-atom simulations [68]. The chemical specificity preserved by this approach allows us to make direct comparisons to the mixed micelle experimental studies by Dubin and coworkers [32]. To facilitate the calculation of *equilibrium* micelle properties we transform the coarse-grained particle-based model into field-theoretic form [69]. This alternative representation of the same particle-based model provides facile access to the free energy, and has been used to evaluate micelle properties and self-assembled morphologies of surfactants [25, 67].

Using this approach, we self-consistently determine the mixed micelle size and morphology in tandem with polyelectrolyte adsorption. Subsequently, we show that the adsorption of polyelectrolytes to micelles correlates well with experimental measures of turbidity, and our model correctly predicts the effect of salt concentration and nonionic surfactant identity. The proposed simulation strategy facilitates the rigorous determination of equilibrium micelle structures, which is challenging to achieve in particle-based simulations, while considering the intricate balance of interactions among all components present in the solution. This establishes a basis for examining complexation propensity in other polyelectrolyte-surfactant mixtures, enabling efficient exploration of formulation space. In Section 2 we describe the computational details and methods of the entire workflow. Subsequently in Section 3 we present the predictions of the model on the behavior of polyelectrolyte-micelle systems upon titration with iso-ionic solutions of the anionic SDS as well as morphological transitions at increasing surfactant concentrations. Finally, in Section 4 we summarize our findings and discuss considerations for future work.

2 Computational details and methods

2.1 All-atom simulations

We parameterize the pair-wise interactions and bonded interactions for the eight coarse-grained (CG) bead types (Fig. 1, first panel) via four stages based on nine reference all-atom (AA)

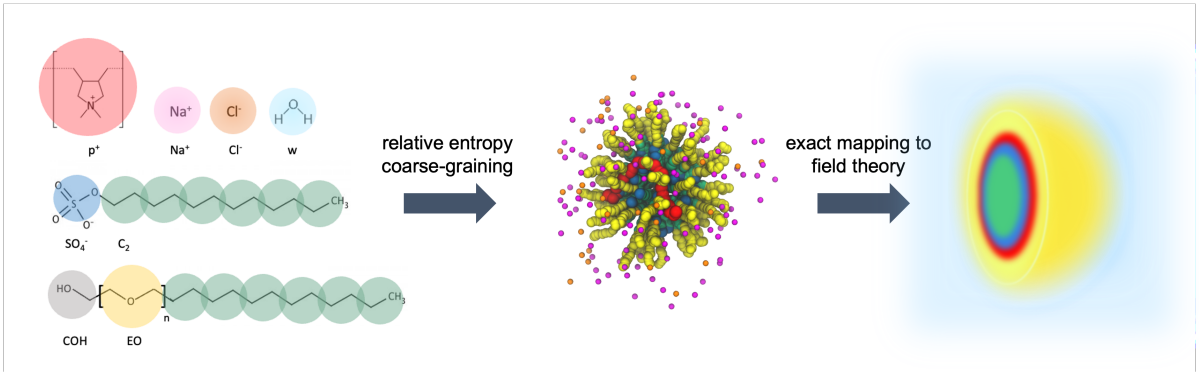

Fig. 1 Schematic of the multi-scale simulation workflow that bridges the all-atom and field theory models. The left panel lists the components we consider in this work. From left to right and top to bottom, chemical structures of the polycation PDADMA monomer, Na^+, Cl^-, water, anionic surfactant SDS and non-ionic surfactant $C_{13}EO_n$ overlaid by the corresponding coarse-grained bead types. The middle panel shows a coarse-grained model parameterized by relative entropy minimization, while the right panel shows the exact mapping from a coarse-grained particle-based description of a PDADMA-SDS/$C_{13}EO_n$ mixed micelle complex to a field-theoretic model (cross-section of the micelle).

simulations as presented in Fig. 2. We use the Optimal Point Charge (OPC) 4-point water model [70] and the Joung-Cheatham ion model [71]. For the PDADMA and the ethylene oxide block on $C_{13}EO_7$, we use the General Amber Force field (GAFF2) [72]. We model the alkyl block (appearing in SDS, $C_{13}EO_7$, and dodecane) with the Lipid 14 force field [73]. We adopt the same force field used in our previous work for the headgroup sulfate SO_4^- [67], which combines the parameters from Yan *et al.* (2010) [74] and subsequently adjusted nonbonded Lennard Jones interaction between sodium ions and oxygens bound to the sulfate headgroup to reproduce the surface tension of SDS deposited at a water-vacuum interface.

We conduct reference AA simulations with the OpenMM simulation package [75]. We use a 1 nm cutoff for the direct space non-bonded interactions and use the Particle Mesh Ewald method to compute long range Coulomb and Lennard-Jones interactions (LJPME method in OpenMM). In addition, we constrain the length of all bonds that involve a hydrogen atom and employ a time step of $dt = 0.002$ ps. The temperature is set to 298.15 K using the Langevin thermostat with a friction coefficient of 5 ps^{-1}, while the pressure is set to 1 atm using the Monte Carlo barostat that is updated every 25 time steps. We generate the initial configurations for the simulations with the Packmol package [76]. Details of the system sizes are provided in Table S1 in the SI.

2.2 Bottom-up coarse-graining procedure

We have previously detailed our workflow for developing a molecularly informed field theory [65–67], and here only summarize the key points. After performing AA simulations as described in the previous section, we use relative entropy coarse-graining [68] with these as references to derive CG interaction potentials that are amenable to efficient field-theoretic simulations. In our CG interaction model, bonded interactions are described using a harmonic bond potential:

$$\beta U_{b,\alpha\gamma}(r) = \frac{3}{2b_{\alpha\gamma}^2} r^2 \tag{1}$$

where $\beta = 1/k_BT$ and $b_{\alpha\gamma}$ is interpreted as the root-mean-square length of a bond between bead species α and γ. Nonbonded interactions consist of an excluded volume and smeared Coulomb interaction between all site pairs, including bonded pairs:

$$\beta U_{ev,\alpha\gamma} = v_{\alpha\gamma} e^{-r^2/2(a_\alpha^2+a_\gamma^2)} \tag{2}$$

$$\beta U_{el,\alpha\gamma} = \frac{l_B \sigma_\alpha \sigma_\gamma}{r} \operatorname{erf}\left(\frac{r}{2\sqrt{a_\alpha^2/2 + a_\gamma^2/2}}\right) \tag{3}$$

where $v_{\alpha\gamma}$ is the excluded volume strength between bead species α and γ, and a_α and σ_α are the Gaussian regularization length and charge of

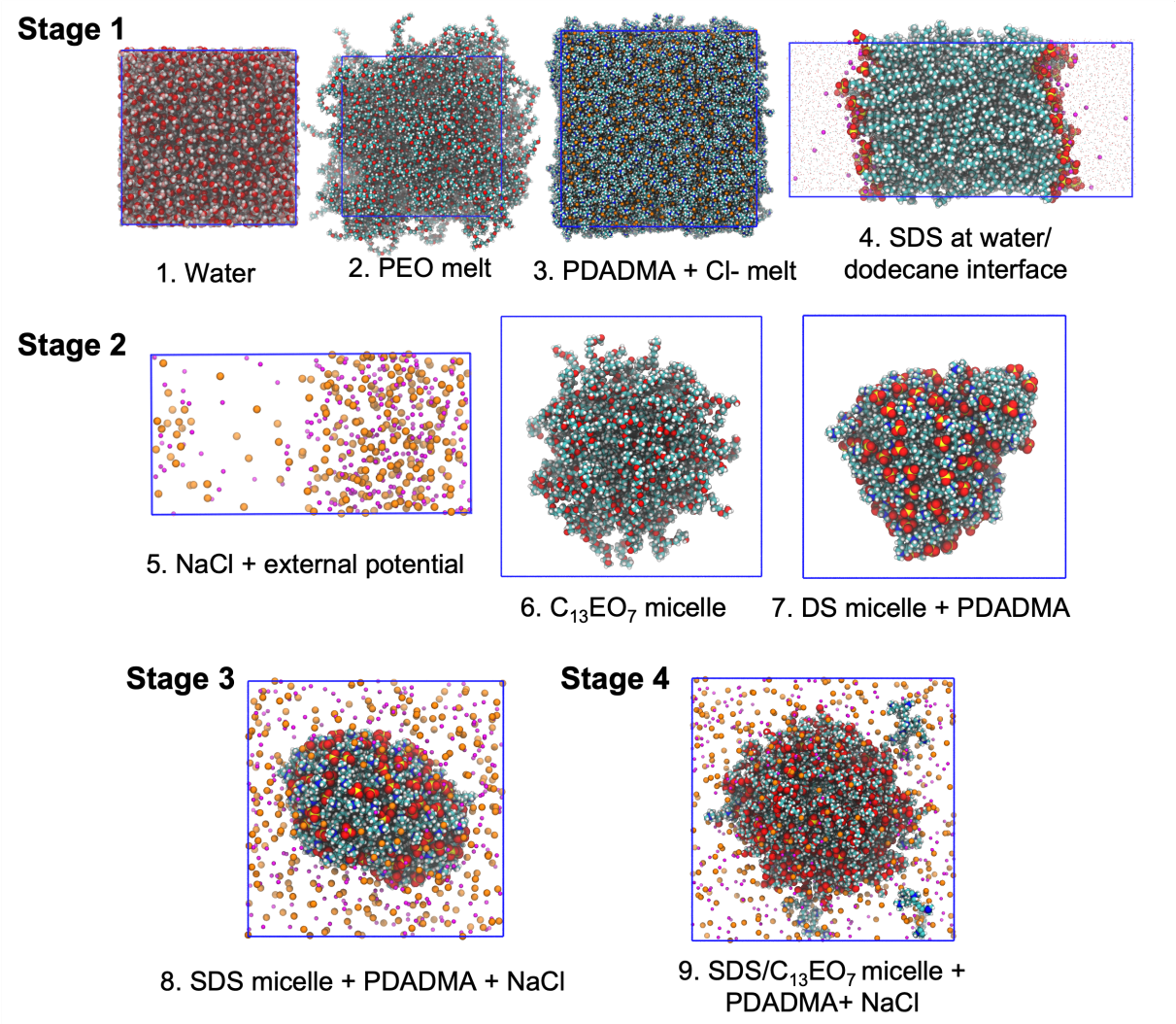

Fig. 2 All-atom simulations used to derived coarse-grained interaction parameters via the relative entropy coarse-graining framework. Simulations details are provided in Table S1

bead species α, respectively. The Bjerrum length l_B charaterizes the strength of the electrostatic interactions and is chosen to be 0.74 nm, which is that of OPC water at 298 K and 1 atm [70]. The smeared Coulomb interaction behaves as an unscreened Coulomb $\sim 1/r$ at large separations r but is regularized to be finite at $r = 0$ to accommodate the soft-core repulsions of the Gaussian repulsive excluded volume potential. Our choice of regularized, soft potentials is physically motivated by the desire to retain long-length-scale physics while coarse-graining over sharp, short-length-scale features [67].

We translate AA reference trajectories for coarse-graining by mapping center-of-mass coordinates of groups of atoms in the AA representation to CG sites. Specifically, we map each water molecule to a single neutral bead and each Na^+ and Cl^- ion to a single bead with $+1$ and -1 charge, respectively. Each monomer of PDADMA is mapped to one bead that bears a $+1$ charge. The 12-carbon alkyl tails on both SDS and $C_{13}EO_n$ are mapped to six neutral C_2 beads of two carbons each. The sulfate head group is represented as a single SO_4^- bead of charge -1. Lastly, the ethylene oxide repeating unit (CH_2OCH_2) on $C_{13}EO_n$ is

mapped to one neutral EO bead and the terminal CH_2OH group is modeled as a neutral COH bead. We fix the Gaussian regularization range, a_α, of each bead species to approximately the cube root of its molecular volume. By this convention, the water interaction range, a_w, is set to 0.31 nm in this work. Values for other bead types are listed in Table S3. The CG bead types and corresponding CG molecules are presented in the first panel of Fig. 1.

We derive CG parameters in successive stages; once the parameters are determined, they are fixed in subsequent steps. In the first stage, we determine CG parameters for the interactions between intramolecular bead species. The water-water repulsion v_{ww} was derived in previous work [66] from pure water AA simulation to reproduce the compressibility of OPC water, $\kappa_T \sim 0.062\ k_BT/a_w^3 \sim 4.51 \times 10^{-10}$ Pa^{-1}. This determines the CG pressure of $P_{CG} = 8.5\ k_BT/a_w^3$ that we use in the subsequent coarse-graining stages. We follow the previously published coarse-graining procedure [67] to parameterize pairwise and bonded interactions for the CG beads in SDS ($v_{C_2\,C_2}$, $v_{SO_4^-\,SO_4^-}$, $v_{C_2SO_4^-}$, v_{C2C_2}, $b_{C_2C_2}$, and $b_{C_2SO_4^-}$) from SDS deposited at a water/dodecane interface at 298.15 K. The EO-EO repulsion $v_{EO\,EO}$ and root-mean-square bond length $b_{EO\,EO}$ are derived using a neat PEO simulation in the NPT ensemble. Similarly, pairwise excluded volume and bonded parameters for the polycation monomer, $v_{p^+p^+}$ and $b_{p^+p^+}$, are also determined from neat PDADMA chains in the NPT ensemble.

In the second stage, we parameterize the ions and cross-interactions involving water as well as those between PDADMA and SDS. We adopt the ion parameters ($v_{Na^+Na^+}$, $v_{Cl^-Cl^-}$, $v_{Na^+Cl^-}$, v_{Na^+w}, and v_{Cl^-w}) from our previous polyelectrolyte work [66] in which we coarse-grained from an aqueous NaCl solution in the external potential ensemble [77]. From the AA simulation of the non-ionic surfactant $C_{13}EO_7$ micelle, we derive the following parameters: $v_{COH\,COH}$, $v_{COH\,C_2}$, $v_{COH\,EO}$, v_{C_2EO}, $v_{COH\,w}$, $v_{C_2\,w}$, $v_{EO\,w}$, b_{C_2EO}, and $b_{COH\,EO}$. Lastly, we determine the cross-interactions among PDADMA, SDS and water ($v_{p^+C_2}$, $v_{p^+SO_4^-}$, v_{p^+w}, $v_{SO_4^-w}$) from a mixture of PDADMA with a SDS micelle.

In stage three, we derive the ions-PDADMA and ions-SDS pair-wise interaction parameters ($v_{p^+Cl^-}$, $v_{p^+Na^+}$, $v_{C_2Cl^-}$, $v_{C_2Na^+}$, $v_{SO_4^-Cl^-}$, and $v_{SO_4^-Na^+}$) from a similar PDADMA and SDS micelle system in the presence of NaCl. In the last stage, the remaining parameters (v_{p^+COH}, v_{p^+EO}, $v_{COH\,Cl^-}$, $v_{COH\,Na^+}$, $v_{COH\,SO_4^-}$, $v_{EO\,Cl^-}$, $v_{EO\,Na^+}$, and $v_{EO\,SO_4^-}$) are derived from a mixture of a SDS/$C_{13}EO_7$ micelle, PDADMA, and NaCl, around the composition range that we target in this study. We tabulate the parameters in Tables S2 and S3.

2.3 Coarse-grained molecular dynamics (CGMD)

CGMD simulations are conducted using a Langevin Dynamics integrator. The Langevin relaxation time τ_{CG} is taken as the unit of time. Due to the soft nature of the CG interactions and bonds, large time steps of 0.1 τ_{CG} are feasible. The inner-loop of relative entropy optimization requires CGMD simulations, which we run for $2 \times 10^5 - 1.5 \times 10^6$ time steps ($2 \times 10^4 - 1.5 \times 10^5$ τ_{CG} of simulation time), sufficient to equilibrate slow relaxation modes in the systems, such as the surface area in the interfacial system used to parameterize SDS interactions with water and salt.

2.4 Micelle simulations with the field theory

One of the primary strengths of the nonbonded CG potentials defined in Section 2.2 is that they can be readily represented and simulated using a field-theoretic representation by means of a Hubbard-Stratonovich-Edwards transformation. This field-theoretic transformation decouples nonbonded pair interactions, resulting in particles interacting only with an auxiliary field. As a result, particle coordinates can be analytically integrated, yielding a partition function in terms of integrals over field configurations:

$$\mathcal{Z} = \int d\mathbf{r}^n e^{-\beta U(\mathbf{r}^n)} \rightarrow \int \mathcal{D}\mathbf{w} e^{-H[\mathbf{w}]} \qquad (4)$$

where H is an effective Hamiltonian describing the statistical weight of the auxiliary field configuration $\mathbf{w}(\mathbf{r})$, and is systematically described elsewhere [69]. It should be emphasized that $\mathbf{w}$ represents a set of auxiliary fields that is sufficient

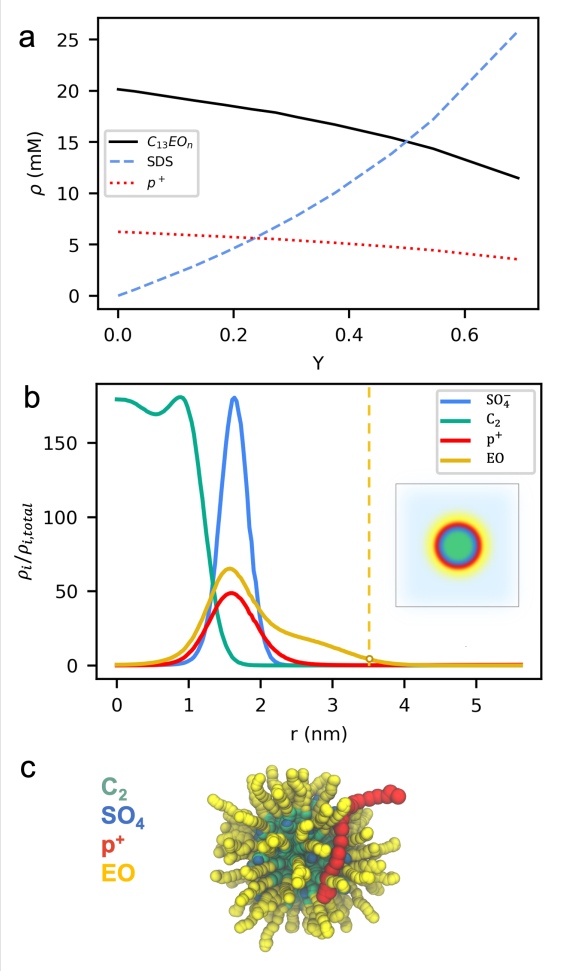

Fig. 3 (a) Concentrations of SDS (chain basis), $C_{13}EO_n$ (chain basis), and DADMA (monomer basis) as the titration proceeds. (b) An example density profile and a cross section of the micelle from SCFT. Dashed line indicates the 0.1 EO locus introduced in the main text. A representative snapshot from CGMD is shown in (c).

to decouple all pairwise interactions of the functional forms defined in Section 2.2. As a result, the field-theoretic transformation is *exact* for the coarse-grained model, and full field-theoretic sampling of the partition function is equivalent to performing CGMD. However, one strength of the field-theoretic representation is that it is amenable to a host of analytical tools that facilitate its evaluation, including the mean field approximation, also termed self-consistent field theory (SCFT):

$$\mathcal{Z} \approx e^{-H[\mathbf{w}^*]} \tag{5}$$

where $\mathbf{w}^*$ is the saddle-point value of each auxiliary field, and represents the dominant field configuration contributing to the partition function. SCFT provides a readily-accessible approximation of the free energy, which is a powerful tool for evaluating the relative stability of competing structures particularly in comparison to conventional MD-based methods requiring significant, often intractable efforts to evaluate phase free energies. For example, minimizing the free energy at constant concentration with respect to the simulation cell size allows one to determine equilibrium sizes and aggregation number of molecular self-assemblies. Additionally, one can compare the free energies of different morphologies (e.g., spherical, cylindrical, lamellar) under stress-free conditions to determine the putative equilibrium structure.

In this work, we take advantage of this particular strength of the field-theoretic transformation to characterize the equilibrium self-assemblies of the multi-component polyelectrolyte-surfactant mixture. We perform simulations of micelles at varying compositions as in the titration experiment outlined by Dubin *et al.* (2017) [32]. Briefly, 60 mM SDS in NaCl is added to solutions of 1 g/L PDADMA (with Cl^- counterions), 20 mM $C_{13}EO_n$, and the same NaCl concentration as in the SDS stock solution. As the titration proceeds, the anionic surfactant fraction increases and the composition changes according to Fig. 3a. This fraction is defined by the surfactant number densities as:

$$Y = \frac{\rho_{SDS}}{\rho_{SDS} + \rho_{C_{13}EO_n}}. \tag{6}$$

Fig. 3b presents an example density profile of a micelle from SCFT. A CGMD snapshot of an equivalent particle-based model is shown in 3c. The mixed micelle comprises of the non-ionic surfactant $C_{13}EO_n$ and SDS with an alkyl-rich core and a corona of SO_4^-, EO, and COH groups. At conditions where the micelle surface charge is above a critical value, the density profile shows an enrichment of PDADMA around the peak concentration of the SO_4^- head group, indicating the adsorption of polyelectrolytes on the micelle surface.

We define several variables to characterize surfactant assembly. First, the number density of

PDADMA monomers adsorbed onto the micelle is calculated by summing over their densities $\rho_{p^+,m}$ at mesh points m that are enclosed within a cut-off distance from the micelle center:

$$\rho_{p^+,adsorbed} = \sum_{m \in r=[0,0.1\ EO\ locus]} \rho_{p^+,m} \quad (7)$$

Here, we choose the cut-off distance where the EO density is 10% of its peak value to the right of the peak (dashed line in Fig. 3b); we refer to this as the "0.1 EO locus". We note that results are not very sensitive to the exact choice of this locus, as long as the adsorbed polyelectrolyte layer lies fully within its radius. Consequently, the fraction of adsorbed PDADMA monomers is

$$f_{p^+,adsorbed} = \frac{\rho_{p^+,adsorbed}}{\sum_m \rho_{p^+,m}} \quad (8)$$

The micelle surface charge density is calculated based on contributions from the surfactant only, i.e., SDS and $C_{13}EO_n$. Since SO_4^- is the only charged species, the surface charge density is

$$\sigma = \frac{\sigma_{SO_4^-}}{4\pi r_s^2} \sum_{m \in r=[0,0.1\ EO\ locus]} \rho_{SO_4^-,m} \quad (9)$$

where $\sigma_{SO_4^-} = -1$ e is the charge of SO_4^- bead. The cut-off distance r_s is taken to be at the 0.1 EO locus and is used to estimate the surface area in the normalization factor.

The aggregation numbers for SDS and $C_{13}EO_n$ are

$$N_{agg,SDS} = \Delta V \sum_{m \in r=[0,0.1\ EO\ locus]} \rho_{SO_4^-,m} \quad (10)$$

$$N_{agg,C_{13}EO_n} = \frac{\Delta V}{n} \sum_{m \in r=[0,0.1\ EO\ locus]} \rho_{EO,m} \quad (11)$$

where n is the number of EO beads in each nonionic surfactant molecule. In addition, we measure the core and micelle radii at the 0.1 C_2 and 0.1 EO loci, respectively.

3 Results and discussion

3.1 SDS titration

We assess the the binding between the polyelectrolyte and the surfactant micelle *via* the amount of 100-mer PDADMA chains adsorbed onto the micelle, as defined in Eq. 8, as the SDS mole fraction Y increases during the titration. Fig. 4a shows that the fraction of adsorbed PDADMA relative to the total PDADMA in the simulation box increases with Y for both SDS/$C_{13}EO_{11}$ and SDS/$C_{13}EO_7$ mixed micelle systems in 0.4 M NaCl, indicating more PDADMA binds to the mixed micelles with the addition of SDS to the mixture. This is expected as micelle surface charge density becomes more negative with increasing anionic surfactant mole fraction (Fig. 4b) which strengthens electrostatic interactions. Experimental measurements that infer micelle charge *via* zeta potential measurements also find that the micelle surface charge density increases with increasing SDS content [32].

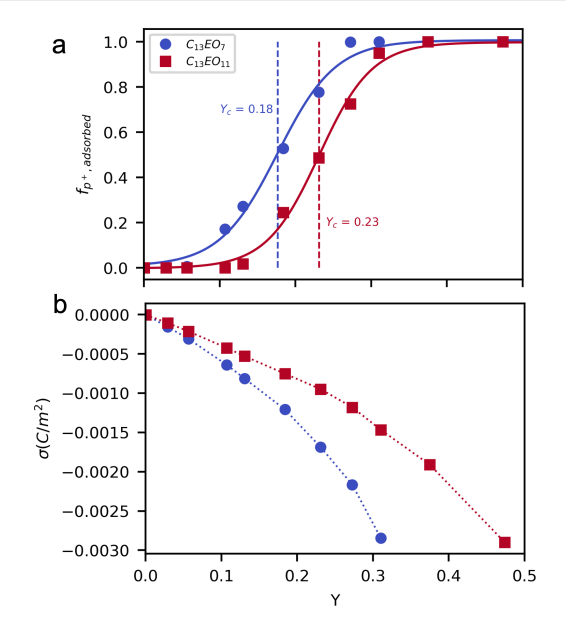

Fig. 4 (a) SCFT-predicted binding isotherms showing the fraction of bound PDADMA (100-mer) as the anionic surfactant mole fraction, Y, increases during the course of the titration at a constant NaCl concentration of 0.4 M for SDS/$C_{13}EO_{11}$ and SDS/$C_{13}EO_7$ micelles. Solid lines are fits to sigmoid functions and Y_c is the Y value at the inflection point. (b) Corresponding micelle surface charge density.

CGMD provides further insight about the interactions between the micelle and polycations. In the first set of CGMD runs, Fig. 5, we initialize a single micelle using the aggregation numbers obtained from SCFT simulations and observe the interaction between a 24-mer PDADMA and the micelle for 2×10^4 τ_{CG}. As expected from SCFT results, PDADMA does not interact with the micelle at $Y = 0$ whereas it adsorbs to the micelle surface when the SDS content increases to $Y = 0.31$. We further investigate the inter-micelle binding at $Y = 0.31$ by doubling the system size to realize two identical micelles and one 48-mer PDADMA. The polycation initially binds to one of the micelles at $t = 0$ and quickly binds to both as the simulation proceeds (Fig. 6a). This inter-micelle binding results in an aggregation of the two micelles, evidenced by the decrease in the center-of-mass distance between them as shown in Fig. 6b. This observation aligns with experimental hypothesis that the increased number of multi-micelle aggregates increases solution turbidity near the onset of complexation [32].

Previous experimental studies [18, 32] have quantified the onset of polyelectrolyte-micelle complexation with the critical composition Y_c, indicated by the initial increase in the turbidity. For comparison, we choose the inflection point of the PDADMA binding isotherms shown in Fig. 4a as Y_c. While this choice is arbitrary, it has relevant implications: complexation is considered to begin when a substantial number of polycation monomers (50% in this case) adsorb onto micelles, and the complexation is detectable through increased turbidity. Notably, the calculated Y_c values from the simulations are 0.18 and 0.23 for SDS/$C_{13}EO_7$ and SDS/$C_{13}EO_{11}$ mixed micelles, respectively, which are in good agreement with the Y_c values of 0.17 and 0.28 from experimental works by Dubin *et al.* (2017, 2018) [18, 32]. Good quantitative (Y_c of SDS/$C_{13}EO_7$) and qualitative (increasing Y_c from SDS/$C_{13}EO_7$ system to SDS/$C_{13}EO_{11}$ system) agreement with experimental results suggests that the Y value at the inflection point of the binding isotherm can reliably describe the onset of complexation observed in previous experimental works. We note that the qualitative trend of SDS/$C_{13}EO_{11}$ micelles exhibiting higher Y_c values than SDS/$C_{13}EO_7$ micelles remains consistent, even when considering other fractions of bound PDADMA as the criteria for the onset of complexation. This agreement

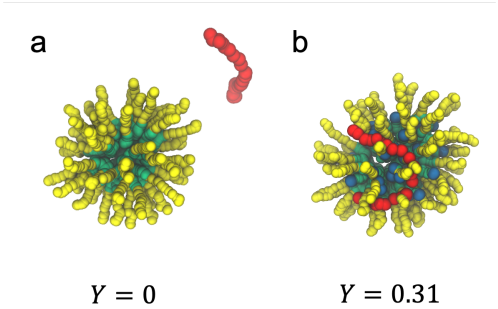

Fig. 5 CGMD snapshots of a single SDS/$C_{13}EO_{11}$ micelle with a 24-mer PDADMA in 0.4 M NaCl at (a) $Y = 0$ (no SDS) and (b) $Y = 0.31$, respectively, with the aggregation numbers taken from SCFT solutions at same conditions. CGMD confirms that PDADMA binds to the micelle at high Y, as suggested by the SCFT binding isotherms. Water and NaCl molecules are not shown for clarity.

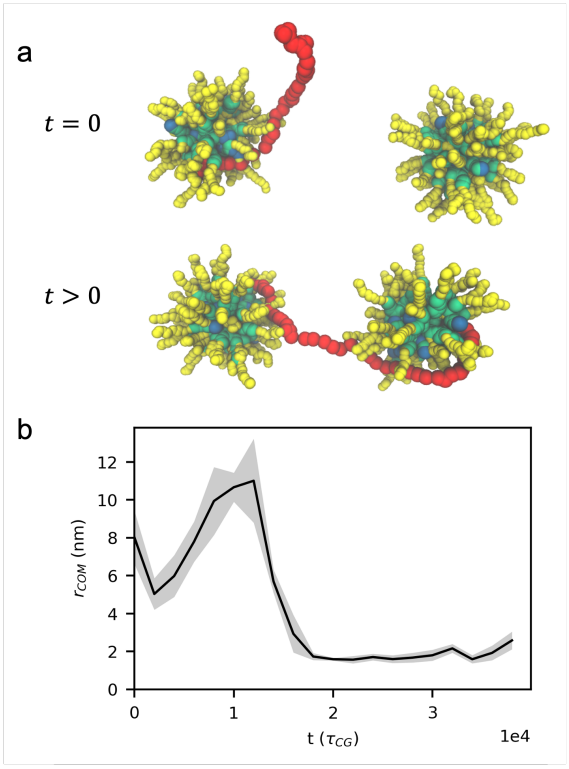

Fig. 6 (a) CGMD snapshots of the same system of Fig. 5b at $Y = 0.31$ but at double the system size with a 48-mer PDADMA. PDADMA initially binds to one micelle $t = 0$ then bridges the two micelles as the simulation proceeds. (b) Center-of-mass distance between the two micelles during the course of the simulation. For reference, the average simulation box size length is 24.3 nm.

helps to validate that our coarse-graining procedure produces a reasonable parameterization of this complex multicomponent system.

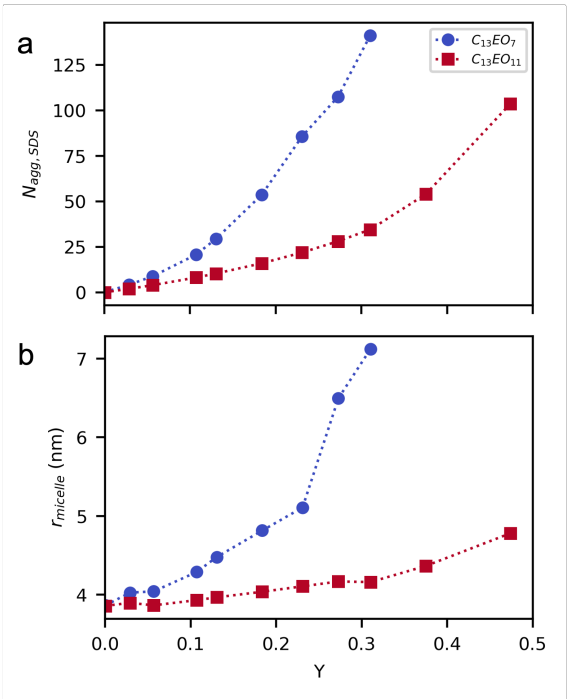

Fig. 7 (a) SDS aggregation number and (b) micelle radius measured at 0.1 EO locus as a function of Y.

Dubin *et al.* [32] defined polyelectrolyte-micelle binding affinity as the resistance of polyelectrolyte-micelle complexes at fixed salt concentration to dissociation by the addition of non-ionic surfactant (decreasing Y), where smaller resistances indicate higher affinity. Thus, from this point of view, lower Y_c in the SDS/$C_{13}EO_7$ system from both simulations and experiments implies that SDS/$C_{13}EO_7$ micelles have higher polyelectrolyte binding affinity than SDS/$C_{13}EO_{11}$ micelles. This is supported by the higher micelle surface charge density when the non-ionic surfactant is $C_{13}EO_7$ (Fig. 4b). At a given value of Y, SDS/$C_{13}EO_7$ micelles have a higher SDS aggregation number $N_{agg,SDS}$ than SDS/$C_{13}EO_{11}$ (Fig. 7a). The radius of the SDS/$C_{13}EO_7$ micelle is also larger than that of the SDS/$C_{13}EO_{11}$ micelle as expected from significantly higher aggregation numbers of SDS and the nonionic ethoxylated surfactant (Fig. S3). Despite having larger surface area, SDS/$C_{13}EO_7$ micelles still have higher surface charge density (Fig. 7b) which leads to stronger electrostatic interactions between PDADMA and SDS/$C_{13}EO_7$ micelles. Interestingly, the critical micelle surface charge density σ_c (σ at the Y_c transition) is more negative for SDS/$C_{13}EO_7$ than SDS/$C_{13}EO_{11}$ (Fig. S2), suggesting higher charged micelles are required for complexation with the former system. We also note that experimentally-reported hydrodynamic radii of the complexes are in the range of 4-8 nm, which is in relatively good agreement with our simulation predictions.

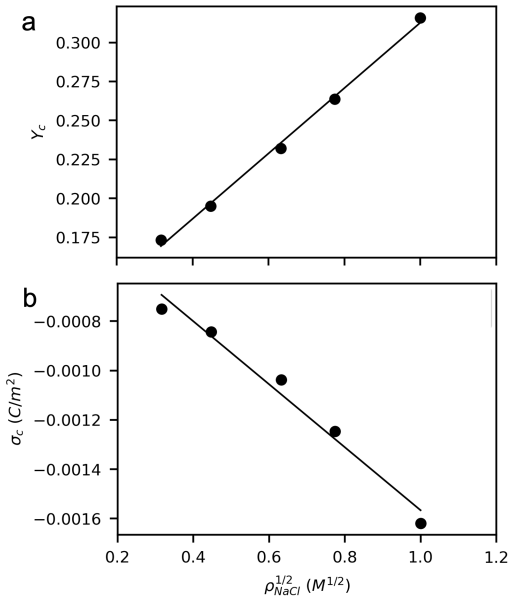

Fig. 8 Dependence of critical (a) SDS content Y_c and (b) micelle surface charge density on added salt concentration. Solids lines are linear regressions with respect to the square root of the salt concentration.

Next, we investigate the effects of salt on the complexation between PDADMA and SDS/$C_{13}EO_{11}$ micelles by repeating the titration procedure at various NaCl concentrations. Fig. 8 presents critical conditions for polyelectrolyte-micelle complexation at added salt concentrations between 0.1 and 1.0 M. While the micelle surface charge density at fixed Y is essentially constant with salt concentration (Fig. S5), the critical SDS content Y_c shifts upward. The increase in Y_c with increasing salt concentration coincides with an increase in the magnitude of the critical micelle surface charge σ_c, which accounts for the salt's

screening of electrostatic interactions. Notably, McQuigg *et al.* has also observed the linear dependence of the critical SDS content, Y_c, and micelle surface charge density σ_c with the square root of the added salt concentration in their experimental study of a similar system, PDADMA and SDS/$C_{12}EO_6$ micelles [78]. According to their simplified model for the binding of a polyelectrolyte to an oppositely charged colloid, such scaling arises when the electrostatic potential in the vicinity of the colloidal particle is less than 0.5 k_BT and the colloidal radius is large relative to the Debye length. As shown in Fig. S7, the electrostatic potential at the 0.1 EO locus in our work is also less than 0.5 k_BT, and the micelle radius, either the core or total micelle radius (Fig. S6c, d), is consistently larger by a factor of ∼2-10 than the Debye length, which varies from 0.96 to 0.30 nm in the 0.1-1.0 M salt concentration range. This implies that McQuigg's simplified model offers a reasonable representation of the micelles in our study, and the consistency in the scaling is justifiable.

3.2 Mesophase transitions

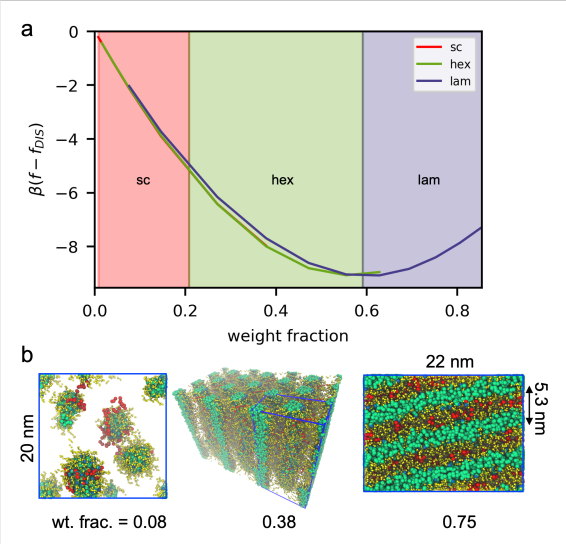

Fig. 9 (a) SCFT free energy densities for mixtures of PDADMA and SDS/$C_{13}EO_{11}$ micelles in 0.4 M NaCl at $Y = 0.3$ and stoichiometric charge. The considered phases are simple cubic sphere (sc), hexagonal cylinder (hex), and lamellae (lam). The disordered free energy is used as reference values. (b) CGMD snapshots at solid (PDADMA, SDS, and $C_{13}EO_{11}$) weight fractions 0.08, 0.38, and 0.75.

So far, we have demonstrated that the CG model presented here shows good agreement with experimental observations for the binding of PDADMA and SDS/$C_{13}EO_n$ micelles in the low concentration regime. Next, we utilize field theory to determine self-assembled structures across a larger range of compositions for mixtures of PDADMA and SDS/$C_{13}EO_{11}$ micelles in 0.4 M NaCl. We set the SDS mole fraction to a fixed value of $Y = 0.3$ and maintain a charge stoichiometry of 1 between PDADMA and SDS. Then, we search for stable phases at increasing weight fractions of PDADMA, SDS, and $C_{13}EO_{11}$. As detailed elsewhere, the free energy density for a given mesophase, which can be directly accessed in SCFT, is minimized with respect to the simulation cell size [79]. A structure is stable when its free energy density is the lowest relative to other candidate structures as well as the homogeneous disordered phase. Here, we consider three phases: simple cubic spheres, hexagonal cylinder, and lamellae (Fig. 9).

Fig. 9a presents free energy densities of these three phases relative to that of the homogeneous disordered phase. At low weight fractions, less than 0.21 weight fraction, SCFT predicts the stable structure is simple cubic with discrete micelles. When fluctuations are included, i.e., in CGMD, unbinding of the lattice occurs and and we observe a solution of spherical micelles (Fig. 9b). Previous assessments of polyelectrolyte-micelle binding reported in Section 3.1 lie in this regime. As the concentration increases above 0.21 weight fraction, we cross over to a region where infinitely long cylindrical structures are stable. Since fluctuations are not included in SCFT, the infinitely long hexagonal cylindrical structure serves as an idealized estimate to an elongated micelle, and can correspond to both wormlike micelles as well as well-ordered hexagonal cylinder phases. Nevertheless, the infinitely long cylinder is a reasonable approximation, as evidenced by the CGMD snapshot of elongated micelles at 0.38 weight fraction. Lastly, lamellar structures, which are also captured in CGMD, are predicted to form above 0.59 weight fraction. This overall sequence of microstructures follows fairly standard, commonly-reported sequences (solution of spherical/rod micelles → ordered cubic and/or

cylindrical phases → lamellar structures) in other surfactant systems [67, 80].

4 Conclusions and outlook

In this work, we have developed a molecularly informed field theory that faithfully describes the complexation behavior between polyelectrolytes and micelles. The model uses relative-entropy minimization to systematically coarse-grain from all-atom simulations. The resulting coarse-grained models are then transformed into a field-theoretic description, which enables rapid self-consistent field-theoretic simulations. Most importantly, field-theoretic simulations allow for direct the evaluation of free energies, and hence the rigorous determination of equilibrium micelle size and structure. In turn, we were able to show how self-assembled micelles change over varying compositions of the nonionic and ionic surfactants, the polyelectrolyte, and salts. Such calculations are possible but much more difficult to perform accurately with equivalent particle-based representations owing to long time scales associated with micelle equilibration processes. Using our workflow, we were able to build a fully-parameterized model of the same molecular system considered by Dubin *et al.* [32] and studied how *mixed micelle* size and properties can change dramatically as surfactant concentration and mixing ratios change along experimental titration paths. Additionally, at high surfactant concentrations, we were also able to locate morphological transitions to cylindrical and lamellar structures to confirm that, for the system under consideration, no cylindrical micelles are expected for the titration paths we considered.

We found that the degree of polyelectrolyte adsorption correlated well with experimentally observed turbidity transitions that announce the onset of polyelectrolyte-micelle complexation. The turbidity transition was also estimated to within 5% of the experimentally reported anionic surfactant mole fraction. Additionally, our model correctly predicts that nonionic ethoxylated surfactants with shorter hydrophilic groups undergo complexation transitions at lower mixing ratios of anionic to nonionic surfactants. While ethoxylated surfactants with shorter head groups tend to form larger micelles than their counterparts with longer head groups, the micelles formed from ethoxylated surfactants with shorter head groups also exhibit higher surface charge density, thus explaining their stronger interaction with polyelectrolytes. Lastly, the critical mole ratio of anionic surfactants and surface charge density of micelles were shown to vary linearly with the square root of salt concentration, in agreement with experimental observations [78].

In conclusion, we have demonstrated that molecularly informed field theories are a powerful tool for exploring the self-assembly of multi-component systems like polyelectrolyte-surfactant mixtures. These field theories have the potential to be chemically specific and allow direct comparison with experiment. Using this tool, we studied how equilibrium self-assemblies of mixed micelles change with solution mixing conditions, and found that polyelectrolyte adsorption curves correlate well with experimental turbidity curves and the onset of soluble polyelectrolyte-micelle complexes. Although previous work [67] and the semi-quantitative agreement with experiments validate that the mean-field approximation used in this work is qualitatively good to describe surfactant self-assembly, including fluctuation effects could further improve predictions of the field-theoretic model. Within the confines of field theory, composition fluctuations that are ignored in the mean-field approximation could be incorporated using techniques such as complex Langevin sampling [69, 81]. By fully sampling the partition function, complex Langevin recovers the same thermodynamic properties as CGMD while retaining rapid equilibration. However, while collective variables like the density are readily accessed within a field theoretic simulation, single-molecule properties require more care [82]. In this study, we focused on investigating the soluble polyelectrolyte-surfactant complexes which only covers a small region of a much richer phase diagram in these systems [17]. Future work can extend this study and rigorously determine phase boundaries in biphasic regions with complex coacervation between polyelectrolytes and surfactants [66].

Supplementary information. Provides details on all-atom simulations, coarse-grained interaction parameters, and additional figures from self-consistent field theory.

Acknowledgments. This work was supported by BASF Corporation through the California Research Alliance. We thank Keith Gutowski for generously sharing papers and engaging in insightful discussions with us. G.H.F. and K.T.D. also derived partial support from the National Science Foundation CMMT Program under grant number DMR-2104255. M.S.S. acknowledges funding support from the National Science Foundation through Award No. CHEM-1800344. K.S. also received support from the BioPACIFIC Materials Innovation Platform (NSF DMR-1933487). Use was made of computational facilities purchased with funds from the National Science Foundation (OAC-1925717) and administered by the Center for Scientific Computing (CSC). The CSC is supported by the California NanoSystems Institute and the Materials Research Science and Engineering Center (MRSEC; NSF DMR-1720256) at UC Santa Barbara.

Declarations

- **Conflict of interest** The authors declare no conflict of interests.
- **Availability of data and materials** The datasets generated during and/or analyzed during the current study are available from the corresponding author on reasonable request.
- **Authors' contributions** My Nguyen and Kevin Shen contributed to the conception, data acquisition and analysis, and writing of the manuscript. Nicholas Sherck, Stephan Köhler, Rohini Gupta, Kris T. Delaney, M. Scott Shell, and Glenn H. Fredrickson contributed to the conception, review and editing of the manuscript, and funding acquisition.

References

[1] E. Goddard, Polymer/surfactant interaction—its relevance to detergent systems. Journal of the American Oil Chemists' Society **71**(1), 1–16 (1994)

[2] K. Bali, Z. Varga, A. Kardos, I. Varga, T. Gilanyi, A. Domjan, A. Wacha, A. Bota, J. Mihaly, R. Meszaros, Effect of dilution on the nonequilibrium polyelectrolyte/surfactant association. Langmuir **34**(48), 14652–14660 (2018)

[3] R. Bradbury, J. Penfold, R.K. Thomas, I.M. Tucker, J.T. Petkov, C. Jones, Manipulating perfume delivery to the interface using polymer–surfactant interactions. Journal of colloid and interface science **466**, 220–226 (2016)

[4] N. Kristen, R. von Klitzing, Effect of polyelectrolyte/surfactant combinations on the stability of foam films. Soft Matter **6**(5), 849–861 (2010)

[5] S. Llamas, E. Guzman, F. Ortega, N. Baghdadli, C. Cazeneuve, R.G. Rubio, G.S. Luengo, Adsorption of polyelectrolytes and polyelectrolytes-surfactant mixtures at surfaces: A physico-chemical approach to a cosmetic challenge. Advances in colloid and interface science **222**, 461–487 (2015)

[6] C.G. De Kruif, F. Weinbreck, R. de Vries, Complex coacervation of proteins and anionic polysaccharides. Current opinion in colloid & interface science **9**(5), 340–349 (2004)

[7] V. Tolstoguzov, Some physico-chemical aspects of protein processing in foods. multicomponent gels. Food Hydrocolloids **9**(4), 317–332 (1995)

[8] F. Weinbreck, R. De Vries, P. Schrooyen, C. De Kruif, Complex coacervation of whey proteins and gum arabic. Biomacromolecules **4**(2), 293–303 (2003)

[9] K.S. Mayya, A. Bhattacharyya, J.F. Argillier, Micro-encapsulation by complex coacervation: Influence of surfactant. Polymer International **52**(4), 644–647 (2003)

[10] Y.V. Shulevich, T.H. Nguyen, D.S. Tutaev, A.V. Navrotskii, I.A. Novakov, Purification of fat-containing wastewater using polyelectrolyte–surfactant complexes. Separation and Purification Technology **113**, 18–23 (2013)

[11] M. Singh, M. Briones, G. Ott, D. O'Hagan, Cationic microparticles: a potent delivery system for dna vaccines. Proceedings of the National Academy of Sciences **97**(2), 811–816 (2000)

[12] K. Hayakawa, J.C. Kwak, Surfactant-polyelectrolyte interactions. 1. binding of dodecyltrimethylammonium ions by sodium dextransulfate and sodium poly (styrenesulfonate) in aqueous solution in the presence of sodium chloride. The Journal of Physical Chemistry **86**(19), 3866–3870 (1982)

[13] K. Hayakawa, J.C. Kwak, Study of surfactant-polyelectrolyte interactions. 2. effect of multivalent counterions on the binding of dodecyltrimethylammonium ions by sodium dextran sulfate and sodium poly (styrene sulfonate) in aqueous solution. The Journal of Physical Chemistry **87**(3), 506–509 (1983)

[14] N. Khan, B. Brettmann, Intermolecular interactions in polyelectrolyte and surfactant complexes in solution. Polymers **11**(1), 51 (2018)

[15] M. López-López, P. López-Cornejo, V.I. Martín, F.J. Ostos, C. Checa-Rodríguez, R. Prados-Carvajal, J.A. Lebrón, P. Huertas, M.L. Moyá, Importance of hydrophobic interactions in the single-chained cationic surfactant-dna complexation. Journal of colloid and interface science **521**, 197–205 (2018)

[16] K. Thalberg, B. Lindman, K. Bergfeldt, Phase behavior of systems of polyacrylate and cationic surfactants. Langmuir **7**(12), 2893–2898 (1991)

[17] Y. Wang, K. Kimura, Q. Huang, P.L. Dubin, W. Jaeger, Effects of salt on polyelectrolyte-micelle coacervation. Macromolecules **32**(21), 7128–7134 (1999)

[18] A.Y. Xu, E. Kizilay, S.P. Madro, J.Z. Vadenais, K.W. McDonald, P.L. Dubin, Dilution induced coacervation in polyelectrolyte–micelle and polyelectrolyte–protein systems. Soft Matter **14**(12), 2391–2399 (2018)

[19] L. Chiappisi, I. Hoffmann, M. Gradzielski, Complexes of oppositely charged polyelectrolytes and surfactants–recent developments in the field of biologically derived polyelectrolytes. Soft Matter **9**(15), 3896–3909 (2013)

[20] A.M. Benhur, J. Diaz, S. Amin, Impact of polyelectrolyte-surfactant interactions on the rheology and wet lubrication performance of conditioning shampoo. International Journal of Cosmetic Science **43**(2), 246–253 (2021)

[21] I.S. Chronakis, P. Alexandridis, Rheological properties of oppositely charged polyelectrolyte- surfactant mixtures: effect of polymer molecular weight and surfactant architecture. Macromolecules **34**(14), 5005–5018 (2001)

[22] L. Maibaum, A.R. Dinner, D. Chandler, Micelle formation and the hydrophobic effect. The Journal of Physical Chemistry B **108**(21), 6778–6781 (2004)

[23] N. Jain, S. Trabelsi, S. Guillot, D. McLoughlin, D. Langevin, P. Letellier, M. Turmine, Critical aggregation concentration in mixed solutions of anionic polyelectrolytes and cationic surfactants. Langmuir **20**(20), 8496–8503 (2004)

[24] J.J. Madinya, C.E. Sing, Hybrid field theory and particle simulation model of polyelectrolyte–surfactant coacervation. Macromolecules **55**(6), 2358–2373 (2022)

[25] T. Wallin, P. Linse, Polyelectrolyte-induced micellization of charged surfactants. calculations based on a self-consistent field lattice model. Langmuir **14**(11), 2940–2949 (1998)

[26] Y. Li, P.L. Dubin, H.A. Havel, S.L. Edwards, H. Dautzenberg, Complex formation between polyelectrolyte and oppositely charged mixed micelles: soluble complexes vs coacervation. Langmuir **11**(7), 2486–2492 (1995)

[27] M. Antonietti, J. Conrad, A. Thuenemann, Polyelectrolyte-surfactant complexes: a new type of solid, mesomorphous material. Macromolecules **27**(21), 6007–6011 (1994)

[28] Y. Lapitsky, E.W. Kaler, Surfactant and polyelectrolyte gel particles for encapsulation and release of aromatic oils. Soft Matter **2**(9), 779–784 (2006)

[29] L.M. Bergström, U.M. Kjellin, P.M. Claesson, I. Grillo, Small-angle neutron scattering study of mixtures of cationic polyelectrolyte and anionic surfactant: Effect of polyelectrolyte charge density. The Journal of Physical Chemistry B **108**(6), 1874–1881 (2004)

[30] M. Gradzielski, I. Hoffmann, Polyelectrolyte-surfactant complexes (pescs) composed of oppositely charged components. Current Opinion in Colloid & Interface Science **35**, 124–141 (2018)

[31] M. Goswami, J.M. Borreguero, P.A. Pincus, B.G. Sumpter, Surfactant-mediated polyelectrolyte self-assembly in a polyelectrolyte–surfactant complex. Macromolecules **48**(24), 9050–9059 (2015)

[32] Y. Fan, M. Kellermeier, A.Y. Xu, V. Boyko, S. Mirtschin, P.L. Dubin, Modulation of polyelectrolyte–micelle interactions via zeta potentials. Macromolecules **50**(14), 5518–5526 (2017)

[33] D. Li, M.S. Kelkar, N.J. Wagner, Phase behavior and molecular thermodynamics of coacervation in oppositely charged polyelectrolyte/surfactant systems: A cationic polymer jr 400 and anionic surfactant sds mixture. Langmuir **28**(28), 10348–10362 (2012)

[34] G.B. Messaoud, L. Promeneur, M. Brennich, S.L. Roelants, P. Le Griel, N. Baccile, Complex coacervation of natural sophorolipid bolaamphiphile micelles with cationic polyelectrolytes. Green Chemistry **20**(14), 3371–3385 (2018)

[35] F. Guillemet, L. Piculell, Interactions in aqueous mixtures of hydrophobically modified polyelectrolyte and oppositely charged surfactant. mixed micelle formation and associative phase separation. The Journal of Physical Chemistry **99**(22), 9201–9209 (1995)

[36] A. Svensson, L. Piculell, B. Cabane, P. Ilekti, A new approach to the phase behavior of oppositely charged polymers and surfactants. The Journal of Physical Chemistry B **106**(5), 1013–1018 (2002)

[37] M. Muthukumar, 50th anniversary perspective: A perspective on polyelectrolyte solutions. Macromolecules **50**(24), 9528–9560 (2017)

[38] E. Kizilay, A.B. Kayitmazer, P.L. Dubin, Complexation and coacervation of polyelectrolytes with oppositely charged colloids. Advances in colloid and interface science **167**(1-2), 24–37 (2011)

[39] G. Pandav, V. Pryamitsyn, J. Errington, V. Ganesan, Multibody interactions, phase behavior, and clustering in nanoparticle–polyelectrolyte mixtures. The Journal of Physical Chemistry B **119**(45), 14536–14550 (2015)

[40] M. Antonov, M. Mazzawi, P.L. Dubin, Entering and exiting the protein- polyelectrolyte coacervate phase via nonmonotonic salt dependence of critical conditions. Biomacromolecules **11**(1), 51–59 (2010)

[41] A.C. Obermeyer, C.E. Mills, X.H. Dong, R.J. Flores, B.D. Olsen, Complex coacervation of supercharged proteins with polyelectrolytes. Soft Matter **12**(15), 3570–3581 (2016)

[42] F. Comert, P.L. Dubin, Liquid-liquid and liquid-solid phase separation in protein-polyelectrolyte systems. Advances in Colloid and Interface Science **239**, 213–217 (2017)

[43] P.L. Dubin, M.E. Curran, J. Hua, Critical linear charge density for binding of a weak polycation to an anionic/nonionic mixed micelle. Langmuir **6**(3), 707–709 (1990)

[44] K. Shen, Z.G. Wang, Electrostatic correlations and the polyelectrolyte self energy. The Journal of chemical physics **146**(8), 084901 (2017)

[45] P. Zhang, K. Shen, N.M. Alsaifi, Z.G. Wang, Salt partitioning in complex coacervation of

symmetric polyelectrolytes. Macromolecules **51**(15), 5586–5593 (2018)

[46] K. Shen, Z.G. Wang, Polyelectrolyte chain structure and solution phase behavior. Macromolecules **51**(5), 1706–1717 (2018)

[47] T.K. Lytle, C.E. Sing, Transfer matrix theory of polymer complex coacervation. Soft Matter **13**(39), 7001–7012 (2017)

[48] L.W. Chang, T.K. Lytle, M. Radhakrishna, J.J. Madinya, J. Vélez, C.E. Sing, S.L. Perry, Sequence and entropy-based control of complex coacervates. Nature communications **8**(1), 1273 (2017)

[49] J. Lou, S. Friedowitz, J. Qin, Y. Xia, Tunable coacervation of well-defined homologous polyanions and polycations by local polarity. ACS central science **5**(3), 549–557 (2019)

[50] A.M. Rumyantsev, N.E. Jackson, J.J. De Pablo, Polyelectrolyte complex coacervates: Recent developments and new frontiers. Annual Review of Condensed Matter Physics **12**, 155–176 (2021)

[51] A.M. Rumyantsev, A. Johner, M.V. Tirrell, J.J. de Pablo, Unifying weak and strong charge correlations within the random phase approximation: Polyampholytes of various sequences. Macromolecules **55**(14), 6260–6274 (2022)

[52] A.M. Rumyantsev, O.V. Borisov, J.J. de Pablo, Structure and dynamics of hybrid colloid–polyelectrolyte coacervates. Macromolecules (2023)

[53] R.D. Groot, Electrostatic interactions in dissipative particle dynamics—simulation of polyelectrolytes and anionic surfactants. The Journal of chemical physics **118**(24), 11265–11277 (2003)

[54] J.M. Borreguero, P.A. Pincus, B.G. Sumpter, M. Goswami, Unraveling the agglomeration mechanism in charged block copolymer and surfactant complexes. Macromolecules **50**(3), 1193–1205 (2017)

[55] P. Hansson, Phase behavior of aqueous polyion–surfactant ion complex salts: A theoretical analysis. Journal of colloid and interface science **332**(1), 183–193 (2009)

[56] B. Wen, B. Bai, R.G. Larson, Surfactant desorption and scission free energies for cylindrical and spherical micelles from umbrella-sampling molecular dynamics simulations. Journal of Colloid and Interface Science **599**, 773–784 (2021)

[57] R. Becker, W. Döring, Kinetische behandlung der keimbildung in übersättigten dämpfen. Annalen der physik **416**(8), 719–752 (1935)

[58] J.A. Mysona, A.V. McCormick, D.C. Morse, Mechanism of micelle birth and death. Physical Review Letters **123**(3), 038003 (2019)

[59] E. Aniansson, S.N. Wall, Kinetics of step-wise micelle association. The Journal of Physical Chemistry **78**(10), 1024–1030 (1974)

[60] B.G. Levine, D.N. LeBard, R. DeVane, W. Shinoda, A. Kohlmeyer, M.L. Klein, Micellization studied by gpu-accelerated coarse-grained molecular dynamics. Journal of Chemical Theory and Computation **7**(12), 4135–4145 (2011)

[61] D.N. LeBard, B.G. Levine, P. Mertmann, S.A. Barr, A. Jusufi, S. Sanders, M.L. Klein, A.Z. Panagiotopoulos, Self-assembly of coarse-grained ionic surfactants accelerated by graphics processing units. Soft Matter **8**(8), 2385–2397 (2012)

[62] M. Jonsson, P. Linse, Polyelectrolyte–macroion complexation. i. effect of linear charge density, chain length, and macroion charge. The Journal of Chemical Physics **115**(7), 3406–3418 (2001)

[63] T. Wallin, P. Linse, Monte carlo simulations of polyelectrolytes at charged micelles. 3. effects of surfactant tail length. The Journal of Physical Chemistry B **101**(28), 5506–5513 (1997)

[64] R. Allen, P. Warren, Phase behaviour of oppositely charged polymer/surfactant mixtures. Europhysics Letters **64**(4), 468 (2003)

[65] N. Sherck, K. Shen, M. Nguyen, B. Yoo, S. Kohler, J.C. Speros, K.T. Delaney, M.S. Shell, G.H. Fredrickson, Molecularly informed field theories from bottom-up coarse-graining. ACS Macro Letters **10**(5), 576–583 (2021)

[66] M. Nguyen, N. Sherck, K. Shen, C.E. Edwards, B. Yoo, S. Köhler, J.C. Speros, M.E. Helgeson, K.T. Delaney, M.S. Shell, G.H. Fredrickson, Predicting polyelectrolyte coacervation from a molecularly informed field-theoretic model. Macromolecules (2022)

[67] K. Shen, M. Nguyen, N. Sherck, B. Yoo, S. Köhler, J. Speros, K.T. Delaney, M.S. Shell, G.H. Fredrickson, Predicting surfactant phase behavior with a molecularly informed field theory. Journal of Colloid and Interface Science (2023)

[68] M.S. Shell, Coarse-graining with the relative entropy. Advances in chemical physics **161**, 395–441 (2016)

[69] G. Fredrickson, et al., *The equilibrium theory of inhomogeneous polymers*, vol. 134 (Oxford University Press on Demand, 2006)

[70] S. Izadi, R. Anandakrishnan, A.V. Onufriev, Building water models: a different approach. J. Phys. Chem. Lett. **5**(21), 3863–3871 (2014)

[71] I.S. Joung, T.E. Cheatham III, Determination of alkali and halide monovalent ion parameters for use in explicitly solvated biomolecular simulations. The journal of physical chemistry B **112**(30), 9020–9041 (2008)

[72] J. Wang, M. Wolf Romain, W. Caldwell James, A. Kollman Peter, A. Case David, Development and testing of a general amber force field. Journal of Computational Chemistry **25**(9), 1157–1174 (2004). https://doi.org/10.1002/jcc.20035

[73] C.J. Dickson, B.D. Madej, Å.A. Skjevik, R.M. Betz, K. Teigen, I.R. Gould, R.C. Walker, Lipid14: the amber lipid force field. Journal of chemical theory and computation **10**(2), 865–879 (2014)

[74] H. Yan, S.L. Yuan, G.Y. Xu, C.B. Liu, Effect of ca2+ and mg2+ ions on surfactant solutions investigated by molecular dynamics simulation. Langmuir **26**(13), 10448–10459 (2010)

[75] P. Eastman, J. Swails, J.D. Chodera, R.T. McGibbon, Y. Zhao, K.A. Beauchamp, L.P. Wang, A.C. Simmonett, M.P. Harrigan, C.D. Stern, et al., Openmm 7: Rapid development of high performance algorithms for molecular dynamics. PLoS computational biology **13**(7), e1005659 (2017)

[76] L. Martínez, R. Andrade, E.G. Birgin, J.M. Martínez, Packmol: A package for building initial configurations for molecular dynamics simulations. Journal of computational chemistry **30**(13), 2157–2164 (2009)

[77] K. Shen, N. Sherck, M. Nguyen, B. Yoo, S. Köhler, J. Speros, K.T. Delaney, G.H. Fredrickson, M.S. Shell, Learning composition-transferable coarse-grained models: Designing external potential ensembles to maximize thermodynamic information. The Journal of Chemical Physics **153**(15), 154116 (2020)

[78] D.W. McQuigg, J.I. Kaplan, P.L. Dubin, Critical conditions for the binding of polyelectrolytes to small oppositely charged micelles. The Journal of Physical Chemistry **96**(4), 1973–1978 (1992)

[79] J.L. Barrat, G.H. Fredrickson, S.W. Sides, Introducing variable cell shape methods in field theory simulations of polymers. The Journal of Physical Chemistry B **109**(14), 6694–6700 (2005)

[80] D.J. Mitchell, G.J. Tiddy, L. Waring, T. Bostock, M.P. McDonald, Phase behaviour of polyoxyethylene surfactants with water. mesophase structures and partial miscibility (cloud points). Journal of

the Chemical Society, Faraday Transactions 1: Physical Chemistry in Condensed Phases **79**(4), 975–1000 (1983)

[81] E.M. Lennon, G.O. Mohler, H.D. Ceniceros, C.J. García-Cervera, G.H. Fredrickson, Numerical solutions of the complex langevin equations in polymer field theory. Multiscale Modeling & Simulation **6**(4), 1347–1370 (2008)

[82] J. Lequieu, T. Koeper, K.T. Delaney, G.H. Fredrickson, Extreme deflection of phase boundaries and chain bridging in a (ba) n miktoarm star polymers. Macromolecules **53**(2), 513–522 (2020)